# Microtubule severing by the katanin complex is activated by PPFR-1–dependent MEI-1 dephosphorylation

José-Eduardo Gomes,[1] Nicolas Tavernier,[1] Bénédicte Richaudeau,[1] Etienne Formstecher,[2] Thomas Boulin,[4] Paul E. Mains,[3] Julien Dumont,[1] and Lionel Pintard[1]

[1]Institut Jacques Monod, Centre National de la Recherche Scientifique, UMR 7592, University of Paris Diderot, F-75205 Paris, France
[2]Hybrigenics, 75014 Paris, France
[3]Department of Biochemistry and Molecular Biology, University of Calgary, Calgary, AB T2N 4N1, Canada
[4]Institut de Biologie de l'Ecole Normale Supérieure, F-75230 Paris, France

Katanin is an evolutionarily conserved microtubule (MT)-severing complex implicated in multiple aspects of MT dynamics. In *Caenorhabditis elegans*, the katanin homologue MEI-1 is required for meiosis, but must be inactivated before mitosis. Here we show that PPFR-1, a regulatory subunit of a trimeric protein phosphatase 4 complex, enhanced katanin MT-severing activity during *C. elegans* meiosis. Loss of *ppfr-1*, similarly to the inactivation of MT severing, caused a specific defect in meiosis II spindle disassembly. We show that a fraction of PPFR-1 was degraded after meiosis, contributing to katanin inactivation. PPFR-1 interacted with MEL-26, the substrate recognition subunit of the CUL-3 RING E3 ligase (CRL3^MEL-26^), which also targeted MEI-1 for post-meiotic degradation. Reversible protein phosphorylation of MEI-1 may ensure temporal activation of the katanin complex during meiosis, whereas CRL3^MEL-26^-mediated degradation of both MEI-1 and its activator PPFR-1 ensure efficient katanin inactivation in the transition to mitosis.

## Introduction

Meiosis is a fundamental process in diploid organisms to produce haploid gametes. One particular feature of oogenesis is that meiosis produces a single haploid oocyte, whereas the remaining chromosome sets are discarded into the polar bodies (PB) with little cytoplasm. In both vertebrates and invertebrates, this highly asymmetric cell division relies on the assembly and positioning at the cell cortex of a small anastral meiotic spindle (Fabritius et al., 2011; Dumont and Desai, 2012).

In *Caenorhabditis elegans*, the assembly, function, cortical localization, and size of the meiotic spindle requires the function of katanin, an evolutionarily conserved AAA–ATPase complex with microtubule (MT)-severing activity that consists of a severing enzyme and a regulatory subunit, respectively, called MEI-1 and MEI-2 in *C. elegans* (McNally and Vale, 1993; Hartman et al., 1998; Srayko et al., 2000; Yang et al., 2003; McNally

et al., 2006). Notably, MT severing by the katanin complex is required for limiting spindle size but not for meiotic spindle assembly, which requires MEI-1 MT bundling activity (McNally and McNally, 2011).

Although essential for meiosis, katanin must be rapidly inactivated before mitosis to allow mitotic spindle assembly (Clark-Maguire and Mains, 1994; Kurz et al., 2002). Katanin is inactivated via proteolysis of the MEI-1 subunit, which is targeted for proteasomal degradation by a Cullin 3 RING-based E3-Ligase using the MEL-26 protein as a substrate-recognition subunit (CRL3^MEL-26^; Dow and Mains, 1998; Furukawa et al., 2003; Pintard et al., 2003a,b; Xu et al., 2003). The rapid inactivation of MT-severing activity is critical as mitosis begins within 15 min of meiosis completion (Kemphues et al., 1986; Yang et al., 2003).

Although the role of katanin in MT severing is well established, there is a paucity of information regarding the regulation

The Rockefeller University Press   $30.00
J. Cell Biol. Vol. 202 No. 3   431–439
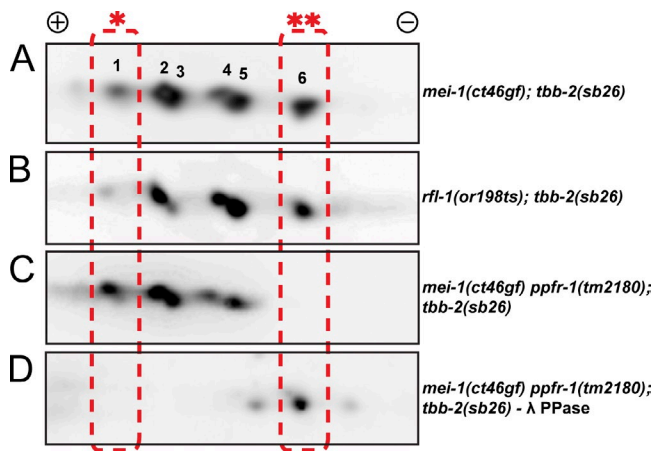www.jcb.org/cgi/doi/10.1083/jcb.201304174

JCB   431

Figure 1. **PPFR-1 regulates MEI-1 phosphorylation status in vivo.** Embryonic extract of the indicated genotypes were analyzed by 2D Western blots using MEI-1 antibodies (*, isoform with highest pI; **, isoform with lowest pI). For all gels, isoelectric focusing is horizontal (positive to the left). (A) Six isoforms were detectable using anti-MEI-1 in *mei-1(ct46gf); tbb-2(sb26)*. (B) The pattern is very similar to A in *rfl-1(or198ts); tbb-2(sb26)*, showing that the MEI-1(P99L) mutation had no effect on the observed isoforms. (C) With *ppfr-1(0)* introduction into the genetic background, the lowest pI isoform (isoform 6) was not detected, whereas the highest pI isoform (isoform 1) was more intense. (D) λ-Phosphatase treatment of extracts of the same genotype as in C.

of its activity. Recent observations revealed that katanin phosphorylation inhibits MT severing in *Xenopus laevis* and this mechanism contributes to interspecies mitotic spindle length scaling (Loughlin et al., 2011). Whether katanin is similarly regulated by phosphorylation in *C. elegans* is unknown, but inactivation of a protein phosphatase 4 complex (PP4), containing the PPH-4.1 catalytic subunit and the PPFR-1/2 regulatory subunits (PP4$^{PPFR-1}$), suppresses *mel-26* and *mei-1(ct46gf)* lethality caused by ectopic MEI-1 activity (Han et al., 2009). Loss of PP4$^{PPFR-1}$ alone causes extrusion of abnormally large PB (Han et al., 2009), suggesting that katanin activity can be regulated through dephosphorylation in *C. elegans*.

# Results and discussion

## PPFR-1 regulates MEI-1 phosphorylation in vivo

To determine biochemically if MEI-1 is a PP4 substrate, we tested whether *ppfr-1* affects MEI-1 phosphorylation in vivo by performing 2D protein electrophoresis from embryonic extracts. To obtain detectable MEI-1 levels, we used the *mei-1(ct46gf)* gain-of-function allele, which encodes the mutated MEI-1(P99L) that is refractory to CRL3$^{MEL-26}$-mediated protein degradation (Pintard et al., 2003b; Xu et al., 2003) or the *rfl-1(or198ts)* in which the CRL3$^{MEL-26}$ E3-ligase is inactivated (Kurz et al., 2002). To render the allelic combinations viable, we included the β-tubulin mutant *tbb-2(sb26)* E439K, which suppresses phenotypes caused by MEI-1 persistence in mitosis (Lu et al., 2004).

As shown in Fig. 1, six distinct MEI-1 isoforms were detected in both *mei-1(ct46gf); tbb-2(sb26)* and *rfl-1(or198ts); tbb-2(sb26)* embryonic extracts, indicating multiple posttranslational modifications. These modifications correspond to different

phosphorylation isoforms because they are undetectable upon λ-phosphatase treatment (Fig. 1 D). Importantly, the least phosphorylated form of MEI-1 (isoform 6) was no longer detected in *ppfr-1(0) mei-1(ct46gf); tbb-2(sb26)* mutant and, conversely, the most negatively charged form (isoform 1) was enriched (Fig. 1 C). Given that PPH-4.1, the catalytic subunit of the phosphatase 4 complex, coimmunoprecipitates with MEI-1 (Han et al., 2009), these results suggest that PP4$^{PPFR-1}$ dephophorylates MEI-1 in vivo.

## *ppfr-1* inactivation enhances a subset of *mei-1* loss-of-function meiotic phenotypes

The fact that *ppfr-1* loss-of-function can suppress *mei-1(ct46gf)* lethality suggests that PPFR-1 could act as a global MEI-1 activator (Han et al., 2009). Alternatively, *ppfr-1* could regulate a subset of MEI-1/katanin functions that are not essential for embryonic viability, such as MT severing. The former hypothesis predicts a strong enhancement of embryonic lethality in *mei-1 ppfr-1* double mutants. To test this prediction, we constructed a strain carrying the *ppfr-1* deletion allele and the temperature-sensitive, loss-of-function allele *mei-1(or646ts)* (henceforth *mei-1(ts)*; O'Rourke et al., 2011). We performed epistasis analysis at a semi-permissive temperature (20°C) and observed 2% ($n = 1,617$) embryonic lethality in *ppfr-1(0)*, 44% ($n = 1,778$) in *mei-1(ts)*, and 39% ($n = 1,765$) in the *mei-1(ts) ppfr-1(0)*. Thus *ppfr-1(0)* does not enhance embryonic lethality of the *mei-1(ts)* hypomorph, suggesting that *ppfr-1* specifically regulates MT-severing activity of MEI-1, which is not essential for viability (McNally and McNally, 2011). Consistent with PPFR-1 regulating a nonessential function of MEI-1, the spindle pole marker ASPM-1 was properly localized and the overall meiotic spindle shape was normal in *ppfr-1(0)* embryos (Fig. S1).

To further demonstrate that PPFR-1 regulates katanin MT-severing activity, we tested if loss of *ppfr-1* could enhance the large PB phenotype of *mei-1(ts)*, which in itself is not lethal (Mains et al., 1990). Consistently, we observed a strong enhancement of the PB size in *mei-1(ts) ppfr-1(0)* embryos compared with either single mutant (Fig. 2 A). Notably, this effect was more severe on the second PB, suggesting that meiosis II (MII) is more sensitive than MI to a reduction in MT severing. Accordingly, reduction of MT severing in the *mei-1(ct46ct103)* mutant or resistance to MT severing in the tubulin *tba-2(sb27); tbb-2(sb26)* double mutant resulted in a second PB that was systematically larger than the first (Fig. 2). Indeed, MT dynamics is substantially different in MI and MII divisions. During MI the spindle is not entirely disassembled and some MTs persist, serving as a seed for the nucleation of new MTs that are incorporated into the MII spindle. In addition, the DNA does not decondense between MI and MII. In contrast, at the end of MII, the DNA decondenses to form the future female pronucleus (PN) and the spindle is fully disassembled, removing all the connections between the female PN and the PB (Fig. S2). MI and MII divisions may thus have different requirements for MT severing. Altogether these results demonstrate that *ppfr-1* positively regulates MEI-1 MT-severing activity during meiosis.

## Loss of *ppfr-1* and MT-severing function causes several meiotic defects

MT bundling and severing activities of MEI-1 can be distinguished with specific separation of function alleles (McNally and McNally, 2011). To address precisely the function of *ppfr-1* and MT severing during MII, we used live-imaging confocal microscopy to visualize MTs (GFP::α-tubulin) and chromosomes (histone 2B::mCherry), in wild type, *ppfr-1(0)*, and MT-severing *mei-1(ct46ct103)* mutant. Compared with wild type, we observed an increase in metaphase and anaphase meiotic spindle length in *mei-1(ct46ct103)* (Fig. 3 A). Chromosomes failed to align properly on the metaphase plate (Fig. 3 A, arrows) and MII spindle poles persisted during anaphase in 100% of embryos (*n* = 12; Fig. 3 B, arrows). Consequently, the spindle was mispositioned at the beginning of anaphase. Whereas the wild-type spindle interacted with the cortex at ∼90°, this angle was severely reduced in *mei-1(ct103ct46)* (Fig. 3 B). We also observed a delay in telophase meiotic spindle disassembly (Fig. 3 C). This phenotype was apparent mainly in MII embryos, which correlates with the observation that only one PB is abnormally larger in MT-severing mutants or in strains resistant to MT severing (*tba-2(sb27); tbb-2(sb26)*; Fig. 2).

Consistent with our hypothesis that PPFR-1 activates MT severing during meiosis, we noticed a slight, yet significant (P < 0.01, *t* test), increase in metaphase and anaphase meiotic spindle length in *ppfr-1(0)* (Fig. 3 A). In addition, MTs persisted around chromatids during anaphase in 82% of embryos (*n* = 17), but this phenotype was not as extreme as in *mei-1(ct46ct103)* embryos, where spindle poles were readily detected while chromatids were separating (Fig. 3 B, arrows). Finally, we also observed a delay in spindle disassembly in *ppfr-1* MII embryos. In 100% (*n* = 11) of wild-type MII embryos, PN detached from the spindle within 6 min after anaphase onset (Fig. 3 C). In contrast, in 41% of *ppfr-1* (*n* = 17), PN chromosomes had not detached from the spindle by 6 min after the beginning of anaphase (Fig. 3 C). *mei-1(ct46ct103)* (*n* = 11) MII embryos presented a similar but more extreme phenotype with the meiotic spindle staying connected to the female PN at the beginning of its migration. However, meiosis occurred at a faster rate in this mutant as compared with wild-type and *ppfr-1(0)* embryos (12 min 50 s ± 60 s [95% CI] and 12 min 20 s ± 70 s [95% CI] from anaphase I to II in wild type and *ppfr-1(0)*, respectively, and 10 min 10 s ± 10 s [95% CI] in *mei-1(ct46ct103)*). Together these results indicate that MT severing contributes to MII spindle disassembly and that PPFR-1 is required for this process.

## PPFR-1 interacts with the substrate-recognition subunit of the CRL3[MEL-26] E3-ligase involved in MEI-1 degradation

Our results indicate that PP4[PPFR-1] dephosphorylates MEI-1 to activate MT severing during meiosis. However, the molecular mechanisms regulating PPFR-1, and more generally protein phosphatase subunits, are poorly understood. Interestingly, we identified PPFR-1 as a binding partner of MEL-26 in two different yeast two-hybrid (Y2H) screens performed with cDNA libraries prepared from either mixed stages or embryos (Fig. 4 A and Table S1).
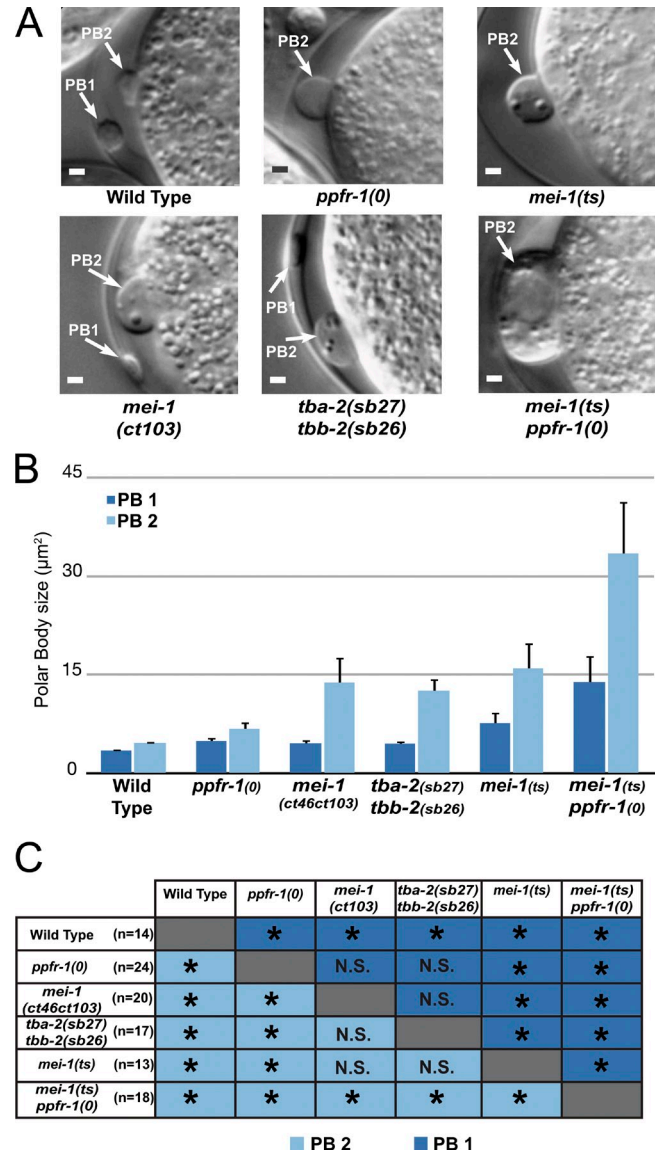


**Figure 2. Large PB phenotype in *ppfr-1(0)*, MT-severing, and MT-severing–resistant mutants.** (A) Nomarski micrographs of PB in wild type, *ppfr-1(0)*, *mei-1(ts)*, *mei-1(ct46ct103)* (MT-severing defective), *tba-2(sb27); tbb-2(sb26)* (resistant to MT severing), and double *ppfr-1(0) mei-1(ts)* at 20°C. Bars, 2 µm. (B) Quantification of PB size as the cross-sectional measurement in the focal plane with the largest area. PB1 and PB2 refer, respectively, to the first and second PB. Error bars, 95% CI. (C) Statistical analysis of the values presented in B: comparison among genotypes of PB1 size (dark blue) and PB2 size (light blue). *, P < 0.01; N.S., not significantly different.

Because PPFR-1 is a MEI-1 activator and rapid MEI-1 inactivation after meiosis is a prerequisite for mitotic spindle assembly, CRL3[MEL-26] might target both MEI-1 and its activator PPFR-1 for degradation to robustly inactivate MT severing after meiosis. Consistent with this possibility, mutation of the substrate-binding interface of MEL-26 (MEL-26 C94Y), which resides in the N-terminal MATH domain, abolished interaction with PPFR-1 in Y2H assays (Fig. 4 B, lane 4).

To confirm Y2H interaction between PPFR-1 and MEL-26, we used pull-down assays. A fraction of 6×His-PPFR-1 C-terminal was retained by immobilized FLAG-MEL-26, but this interaction was much weaker with FLAG-MEL-26 C94Y,

Figure 3. **Live-imaging analysis of MII embryos in wild type, *ppfr-1(0)*, and MT-severing *mei-1* mutants.** (A) Live images of meiotic spindles in metaphase II and anaphase II of wild type, *ppfr-1(0)*, and *mei-1(ct46ct103)* carrying GFP::α-Tubulin (green) and Histone2B::mCherry (red) transgenes. Graphs quantify spindle length. Error bars, 95% CI; **, P < 0.01 (*t* test; metaphase: wild type, *n* = 17; *ppfr-1(0)*, *n* = 32; *mei-1(ct46ct103)*, *n* = 9; anaphase: wild type, *n* = 22; *ppfr-1(0)*, *n* = 36; *mei-1(ct46ct103)*, *n* = 11). Arrows point to lagging chromosomes. Bars, 5 µm. (B, left) Live images of early anaphase II spindles. PB1, first PB. Arrows point to spindle poles that persist in *ppfr-1(0)* and to a larger extent in *mei-1(ct46ct103)* MII embryos. Fractions in the bottom-right of the merge panels refer to the number of embryos showing spindle pole persistence. (right) Schematics of early anaphase II spindle orientation relative to the cell cortex in wild type, *ppfr-1(0)*, and *mei-1(ct46ct103)*. Each blue dash represents a single scored embryo; gray shade represents the range of angles observed from 82° to 89° (*n* = 11) in wild type, 82° to 90° (*n* = 17) in *ppfr-1(0)*, and 15° to 45° (*n* = 11) in *mei-1(ct46ct103)*. (C) Telophase images of live meiotic embryos as in A and B. PN, maternal PN. PB1 and PB2 are the first and second PB, respectively. The fraction of embryos that showed PB chromosomes connected to the PN via the meiotic spindle is indicated at the bottom left of the last frame.
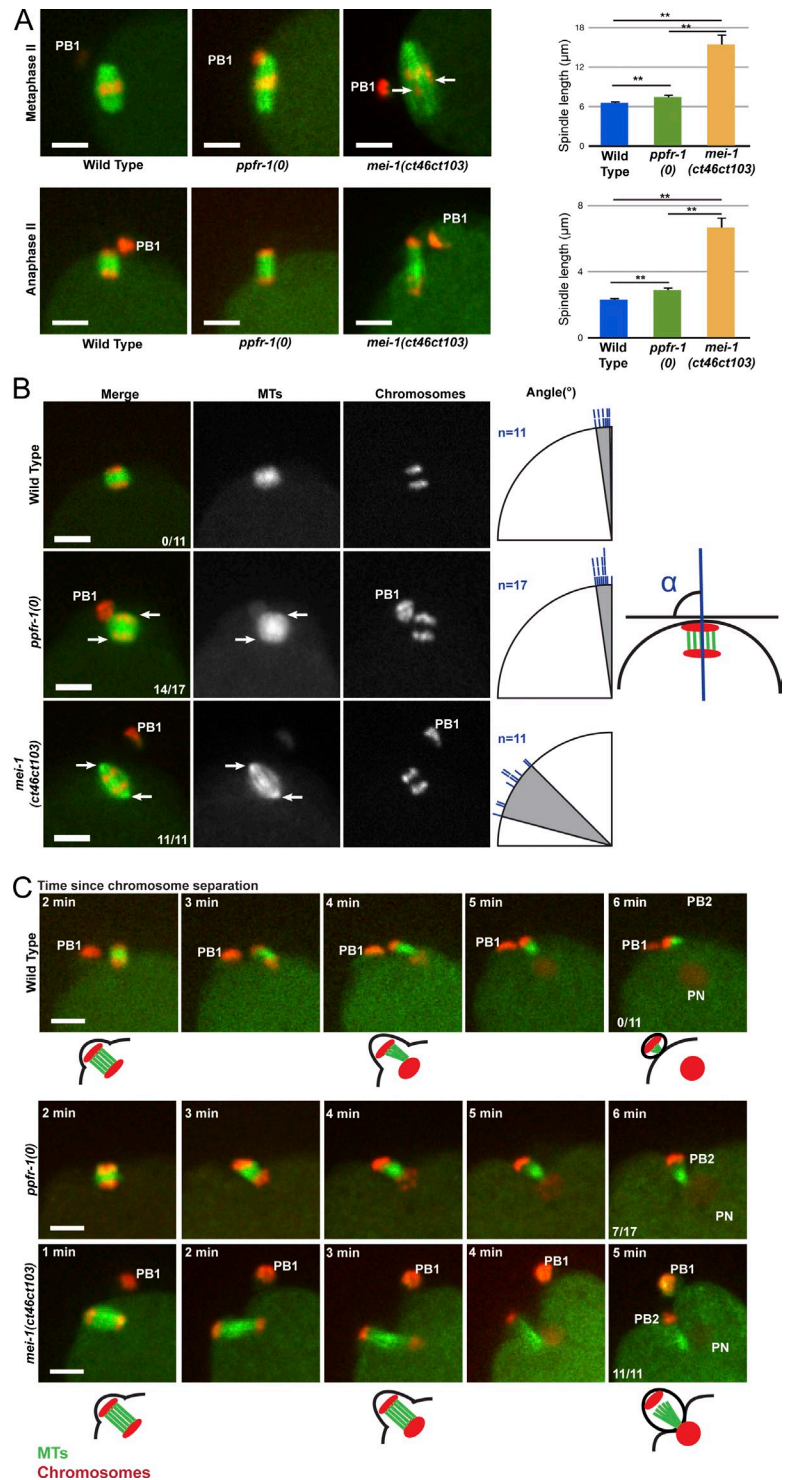


confirming that PPFR-1, like MEI-1, interacts with the MEL-26 MATH domain (Fig. 4 C).

Because both MEI-1 and PPFR-1 bind the MATH domain of MEL-26, we asked if PPFR-1 and MEI-1 share sequence similarities. The minimal common region of interaction among the different PPFR-1 fragments identified in the Y2H screens corresponds to the PPFR-1 C-terminal 117 residues. Indeed the last 32 amino acids of PPFR-1 exhibit sequence similarity with the region of MEI-1 harboring the putative MEL-26 phosphodegron (Fig. 4 A). Importantly, this region contains the P99L of *mei-1(ct46gf)*, which abolishes the MEL-26–MEI-1 interaction, and S92, whose MBK-2 (mini-brain kinase) phosphorylation contributes to MEI-1 degradation in vivo (Stitzel et al., 2006), presumably by promoting interaction with MEL-26. Accordingly, mutated S92A MEI-1 blocked MEL-26 Y2H interactions (Fig. 4 B, lane 8), whereas the phospho-mimicking S92D maintained the interaction (Fig. 4 B, lane 9). We asked if the C-terminal stretch of PPFR-1 might
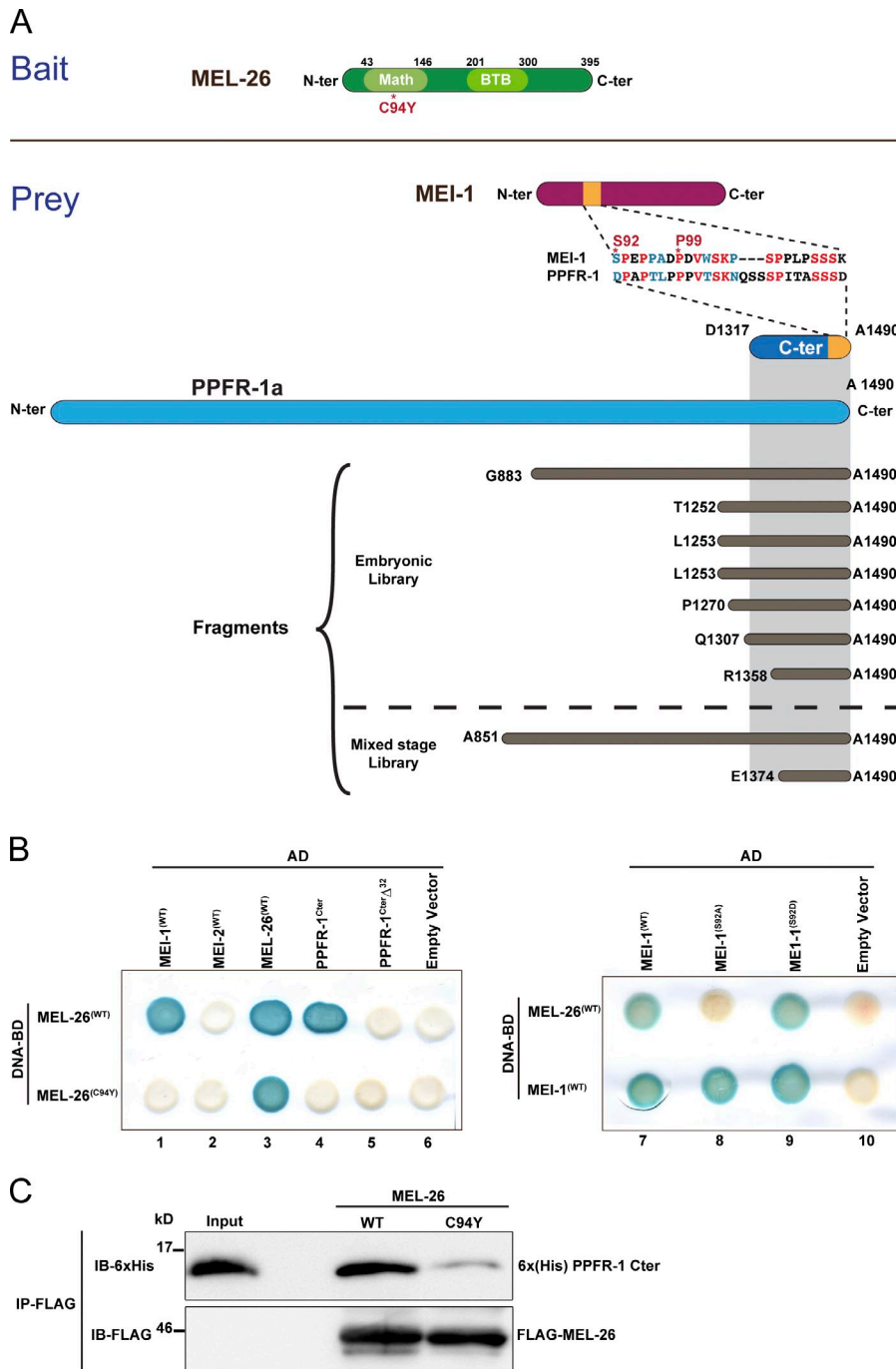
**Bait**

MEL-26  N-ter — 43 · 146 · Math · 201 · BTB · 300 · 395 — C-ter
C94Y

**Prey**

MEI-1  N-ter ——— C-ter
S92   P99

MEI-1    SPEPPADPDVWSKP---SPPLPSSSK
PPFR-1   DPAPTLPPPVTSKNQSSSPITASSSD

D1317 — C-ter — A1490

**PPFR-1a**
N-ter ————————— A1490
C-ter

**Fragments**

Embryonic Library:
G883 ——————— A1490
T1252 ——— A1490
L1253 ——— A1490
L1253 ——— A1490
P1270 ——— A1490
Q1307 ——— A1490
R1358 ——— A1490

Mixed stage Library:
A851 ————————— A1490
E1374 ——— A1490

Figure 4. **PPFR-1 interacts with MEL-26, the CRL3^MEL-26 E3-ligase substrate-recognition subunit.** (A) PPFR-1 was identified as a partner of MEL-26 in two Y2H screens using full-length MEL-26 as bait and random-primed cDNA libraries prepared from mixed stages or embryos. Distinct fragments identified in each screen are shown. (B) The interaction between MEL-26 fused to the Gal4-DNA–binding domain (DNA-BD) was characterized by Y2H assays with MEI-1, MEI-2, MEL-26, and PPFR-1 constructs (amino acids 1317–1490; A, gray shade) fused to the Gal4 activation domain (AD). Positive interaction was scored by β-galactosidase assays. (C) An equal amount of FLAG-MEL-26 or MEL-26(C94Y) produced in insect cells was immobilized on FLAG agarose beads and incubated with bacterially expressed 6×His-PPFR-1 C-terminal (amino acids 1317–1490). Bound proteins were eluted and immunoblotted with PPFR-1 (top) or FLAG antibodies (bottom). 1/20th of the 6×His-PPFR-1 input was loaded for comparison with 1/20th of beads.

**B**

AD: MEI-1(WT) · MEI-2(WT) · MEL-26(WT) · PPFR-1^Cter · PPFR-1^CterΔ32 · Empty Vector

DNA-BD: MEL-26(WT) / MEL-26(C94Y)

1 2 3 4 5 6

AD: MEI-1(WT) · MEI-1(S92A) · MEI-1(S92D) · Empty Vector

DNA-BD: MEL-26(WT) / MEI-1(WT)

7 8 9 10

**C**

IP-FLAG

MEL-26: Input · WT · C94Y
kD
17— IB-6xHis → 6x(His) PPFR-1 Cter
46— IB-FLAG → FLAG-MEL-26

be similarly required for MEL-26 interactions. Indeed, deletion of the last PPFR-1 32 amino acids abolished PPFR-1–MEL-26 interactions (Fig. 4 B, lane 5), suggesting that PPFR-1, like MEI-1, is a CRL3^MEL-26 substrate.

### CRL3^MEL-26 E3-ligase regulates PPFR-1 mitotic protein levels

To further investigate regulation of PPFR-1 by the CRL3^MEL-26 E3-ligase, we evaluated PPFR-1 protein levels in *mel-26(tm1664)* and *cul-3(RNAi)* embryos by Western blots. The PPFR-1 antibody recognized two bands in wild-type embryonic extracts, consistent with the predicted sizes of the PPFR-1a, PPFR-1b, or PPFR-1d predicted splicing isoforms (166, 152, and 178 kD, respectively; Fig. 5 A). In extracts of the deletion allele *mel-26(tm1664)*, the antibody similarly detected two bands of the same molecular masses with a twofold increase in the intensity of the lower band (Fig. 5 A), consistent with one PPFR-1 isoform (a or b) being a CRL3^MEL-26 degradation target. These results were not an indirect consequence of *mel-26(0)* lethality because PPFR-1 similarly accumulated in the viable strain *mel-26(ct61sb4); tbb-2(sb26)* (Fig. 5 A). Likewise PPFR-1a accumulated in *cul-3(RNAi); tbb-2(sb26)*, indicating that CRL3^MEL-26 regulates PPFR-1 embryonic protein levels.

**Figure 5. PPFR-1 accumulates at centrosomes in *mel-26* mutant embryos.** (A) PPFR-1 protein detected on Western blots from embryonic extracts. Two PPFR-1 isoforms were detected with apparent molecular mass consistent with predicted isoforms PPFR-1a (166 kD), PPFR-1b (152 kD), or PPFR-1d (178 kD). Intensity levels normalized relative to control genotype (i.e., in controls PPFR-1a/b to actin ratio = 1). (B) Confocal micrographs of wild-type, *mel-26(tm1664)*, and *mei-1(ct46gf)* embryos, stained for PPFR-1 (green), α-tubulin (red), and DNA (blue). White arrows point to the centrosomes. Bar, 10 µm. (C) Quantification of PPFR-1 staining at anaphase and telophase centrosomes expressed as a percentage of enrichment relative to cytoplasmic level. Wild type, n = 15; *mel-26* n = 8; *mei-1(ct46gf)*, n = 7 (*, P < 0.05; **, P < 0.01; NS, not significant; *t* test). Error bars, 95% CI. (D) The CRL3[MEL-26] E3-ligase targets both MEI-1 and its activator PPFR-1 for degradation to regulate MT severing upon meiotic exit.
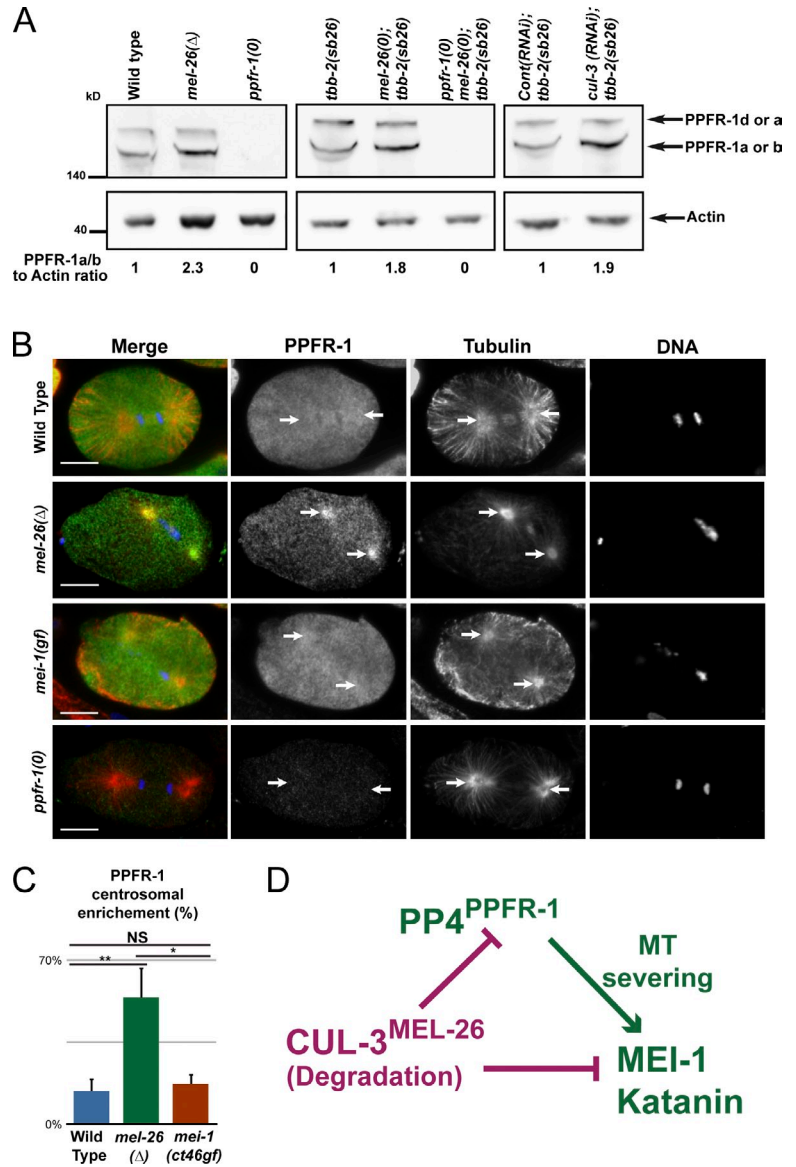


## PPFR-1 and MEI-1 accumulate at centrosomes in *mel-26* mutant embryos

PPFR-1 is homogenously localized throughout the wild-type cytoplasm during both meiosis (Fig. S1 B) and mitosis (Fig. 5 B); however, it accumulates at the centrosomes in *mel-26(tm1664)* null embryos (Fig. 5 B). Because MEI-1 similarly accumulates at centrosomes in *mel-26* mutant embryos (Clark-Maguire and Mains, 1994; Pintard et al., 2003b), increased centrosomal PPFR-1 could result from passive binding of ectopic centrosomal MEI-1, rather than being a direct consequence of defects in MEL-26–mediated PPFR-1 degradation. However, PPFR-1 did not accumulate when the excess MEI-1 at the centrosomes resulted from *mei-1(ct46gf)* (Fig. 4 B). Thus, CRL3[MEL-26] degrades a fraction of PPFR-1 after meiosis, preventing PPFR-1 accumulation at centrosomes. This colocalization with ectopic MEI-1 could enhance MT-severing activity, explaining *ppfr-1(0)* suppression of *mei-1(ct46gf)* and *mel-26* (Han et al., 2009).

In conclusion, our results indicate that PP4[PPFR-1] dephosphorylates MEI-1 to regulate katanin MT-severing activity during meiosis. MT severing is required for increasing net MT mass early in meiosis and for spindle shortening during metaphase and anaphase (McNally et al., 2006; Srayko et al., 2006). Here we confirm these observations and show that MT severing is required for anaphase spindle pole disassembly. In addition, MT severing contributes to MII telophase central spindle disassembly and PPFR-1 regulates this process. Interestingly, Aurora B, the kinase subunit of the chromosomal passenger complex (CPC), phophorylates katanin to inhibit MT severing in *X. laevis* (Loughlin et al., 2011). Although the phosphorylated residue is not conserved in MEI-1, the CPC might still be involved in MEI-1 phosphorylation to regulate meiotic spindle function as the CPC localizes to the chromosomes in metaphase and the meiotic spindle in anaphase and Aurora B/*air-2(−)* embryos present severely disorganized meiotic spindles (Dumont et al., 2010). The CPC might locally inactivate MT severing during metaphase to build a central spindle, whereas MEI-1 dephosphorylation by PP4[PPFR-1] during anaphase would later activate katanin to sever chromosome–MT connections and

disassemble the meiotic spindle. MT-severing activity, however, must be rapidly down-regulated before mitosis and here we show that CRL3$^{MEL-26}$ E3-ligase targets both MEI-1 and its activator PPFR-1 for proteasomal degradation, ensuring an efficient inactivation of katanin before mitosis. This is, to the best of our knowledge, the first example of a phosphatase and its substrate being degraded by the same E3-ligase.

# Materials and methods

### Nematode culture and strains

*C. elegans* strains were cultured and maintained using standard procedures (Brenner, 1974) unless otherwise specified. Temperature-sensitive (ts) strains were upshifted at the L4 stage 24 h before embryos were collected. Embryonic lethality (hatching rate) was scored from the first 6- to 8-h brood of at least 10 hermaphrodites. Strains with the following genotypes were used in this study: N2 (reference strain), *mei-1(ct46gf) unc-29(1072) I*; *tbb-2(sb26) III*, *rfl-1(or198ts) tbb-2 (sb26) III*, *mei-1(ct46gf) unc-29(1072) ppfr-1(tm2180) I*; *tbb-2(sb26) III*, *ppfr-1(tm2180) I*, *mei-1(or646ts) I* (provided by B. Bowerman, University of Oregon, Eugene, OR; O'Rourke et al., 2011), *mei-1(ct46ct103) unc-29(e1072) I*, *mei-1(or646ts) ppfr-1(tm2180) I*, *tba-2(sb27) I*; *tbb-2(sb26) III*, *Histone2B::mCherry(ltIs37) IV*; *GFP::α-tubulin(ltIs25)*, *mei-1(ct46ct103) I*; *Histone2B::mCherry(ltIs37) IV*; *GFP::α-tubulin(ltIs25)*, *ppfr-1(tm2180) I*; *Histone2B::mCherry(ltIs37) IV*; *GFP:: α-tubulin(ltIs25)*, *mel-26(tm1664) I*, *tbb-2(sb26) III*, and *mel-26(ct61sb4) I tbb-2(sb26) III*. Mutations used included the following: (LG1) *mei-1(ct46gf)* gain-of-function allele, *mei-1(ct46ct103)* loss-of-function allele affecting specifically MT severing, *mei-1(or646ts)* temperature-sensitive loss-of-function allele, *mel-26(tm1664)* deletion, *mel-26(ct61sb4)* genetic null allele, *ppfr-1(tm2180)* deletion, *tba-2(sb27)* α-tubulin mutant refractory to Katanin severing, *unc-13(e1091)* and *unc-29(e1072)*, which are uncoordinated and were used as linkage phenotypic markers, *(LGIII) tbb-2(sb26)* β-tubulin mutant refractory Katanin severing, and *rfl-1(or198ts)* temperature-sensitive loss-of-function allele. Descriptions can be found at http://www.wormbase.org. The following transgenes were used: Histone2B::m Cherry *ltIs37* [pAA64; *pie-1*/mCHERRY::*his-58*; *unc-119(+)*] *IV* and GFP::α-tubulin *ltIs25* [pAZ132; *pie-1*/GFP::*tba-2*; *unc-119(+)*] (Dumont et al., 2010). RNAi was performed by feeding as described previously (Kamath et al., 2001). For *cul-3* inactivation, L4 animals were fed for 48 h at 23°C using the *cul-3* clone (Pintard et al., 2003a).

### In vivo imaging of meiotic divisions

Imaging of the meiotic divisions was performed as described previously (Dumont et al., 2010) using a spinning disk confocal microscope. Adult worms were dissected in 4 µl L-15 blastomere culture medium on a 24 × 60-mm coverslip mounted on a metal holder. The drop of medium was surrounded by a ring of petroleum jelly that serves as a spacer, thereby preventing compression of the embryos. A coverslip (18 × 18 mm) was placed on top to seal the chamber and prevent evaporation during filming. Live imaging was performed at 20°C using a spinning disc confocal head (CSU-X1; Yokogawa Corporation of America) mounted on a Ti-E inverted microscope (Nikon) equipped with 491- and 561-nm lasers (Roper Scientific) and a charge-coupled device camera (Coolsnap HQ2; Photometrics). Acquisition parameters were controlled by MetaMorph software (Molecular Devices). In all cases a 60×, 1.4 NA PlanApochromat lens with 2 × 2 binning was used, and four z-sections were collected at 2-µm intervals every 20 s. In Fig. 3, each image shown results from the sum of three adjacent focal planes (performed with ImageJ/Fiji software).

### Immunofluorescence and microscopy

Worms were dissected in either M9 (for mitotic embryos) or blastomere culture solution (for meiotic embryos). Embryos were transferred to subbing solution-coated slides, freeze cracked by flipping off the coverslip after liquid nitrogen freezing, and fixed for 20 min in −20°C methanol. Affinity-purified PPFR-1 antibody (see Protein extracts, antibodies, and immunoblotting section) was used at a dilution of 1:100, monoclonal α-tubulin antibody (Dm1α; Sigma-Aldrich) was used at 1:500, and the secondary antibodies were coupled to the fluorophores Alexa Fluor 488 or Alexa Fluor 543 (Molecular Probes) used at 1:400. Embryos were mounted in Vectashield mounting medium with DAPI. Fixed embryos were imaged on a DM IRB inverted microscope (Leica) or a TCS SP5 confocal microscope (Leica). To assess PB size, live embryos were recorded

at room temperature by time-lapse Nomarski microscopy using an Axioimager microscope (Carl Zeiss), 100× objective, and ICc1 camera (Carl Zeiss) controlled by Axiovision software (Carl Zeiss). The maximal crosssectional area of the PB was measured using Axiovision software. Spindle length, spindle orientation, and fluorescence intensity were measured using Image J/Fiji Software. For spindle length, reslice function was used to allow measurement in 3D. Metaphase length was measured at the earliest moment of chromosome alignment at the metaphase plate. Anaphase length was measured at the moment of maximum distance between chromatids before spindle disassembly.

### Protein extracts, antibodies, and immunoblotting

Embryo extracts were prepared by hypochlorite treatment. Adult worms were bleached, washed three times in M9 buffer, resuspended in 1 vol of 3× Laemmli buffer, and boiled for 5 min at 95°C. Standard procedures were used for SDS-PAGE and Western blotting (Sambrook et al., 1989); 4–12% gradient of polyacrylamide gels were used (Invitrogen).

The noncommercially available polyclonal antibodies used in this study were all raised in rabbits directed against proteins ASPM-1 (provided by S. Van den Heuvel, Developmental Biology, Utrecht, Netherlands; van der Voet et al., 2009), PPFR-1 (this study), and MEI-1 (Pintard et al., 2003b). In brief, the vector pGEX-4T (Pfizer) was used to express GST fusions of PPFR-1 C terminus (from residue D1317 to V1468 of the PPFR-1a sequence) and MEI-1 full-length in *E. coli* BL21 DE3 strain. Inclusion bodies were prepared and loaded onto SDS-PAGE according to standard procedures. Fusion proteins were electroeluted and were used to immunize rabbits. PPFR-1 and MEI-1 antibodies were affinity purified over maltose binding protein–PPFR-1 and –MEI-1 affinity columns, respectively. To prepare the affinity columns, maltose binding protein fusion proteins were expressed in bacteria, purified over amylose resin according to the manufacturer's instructions (New England Biolabs, Inc.), and covalently linked to CNBr-activated Sepharose (Pfizer).

Commercially available antibodies directed against actin (MP Biomedicals) 1:2,000 and the FLAG peptide (Sigma-Aldrich) were used at a dilution of 1:2,000 and 1:1,000, respectively. Secondary antibodies conjugated to peroxidase against rabbit or mouse antibodies were purchased from Sigma-Aldrich and used at 1:3,000.

For FLAG pull-down experiments, FLAG-MEL-26 wild-type and C94Y mutated versions were expressed in Sf9 insect cells and purified using anti-FLAG agarose beads (Sigma-Aldrich). Purified proteins were then incubated at 4°C for 2 h with the C-terminal fragment of PPFR-1, produced and purified from in *E. coli* as an N-terminal fusion with the 6×His Tag, in binding buffer (100 mM Tris-HCl, pH 8, 120 mM NaCl, 1 mM EDTA, and Complete Mini EDTA-free Protease Inhibitor Cocktail [Roche]). Resins were washed four times in binding buffer and resuspended in SDS sample buffer. Proteins bound to the FLAG resins were resolved by SDS-PAGE on a 10% gel. Immunodetection was performed with antisera to PPFR-1 (this study) and FLAG (Sigma-Aldrich).

### 2D gel electrophoresis

2D gel analysis was conducted essentially as described previously (Kitagawa et al., 2009) with 7-cm strips of pH 4.0 to 7 and using a Ettan IPGphor 3 (GE Healthcare). For dephosphorylation, 20 µl of embryonic extract in Laemmli buffer were diluted in λ-phosphatase buffer, supplemented with MnCl$_2$ and 2 µl of λ -phosphatase enzyme added per reaction (New England Biolabs, Inc.) to a final volume of 600 µl. After 6 h at 30°C, proteins were precipitated with TCA (20% final concentration), washed with −20°C cold acetone, resuspended in Destreak buffer (GE Healthcare), and processed for 2D gel analysis as described previously (Kitagawa et al., 2009).

### Statistical analysis

Statistical analysis was performed using Numbers software (Apple).

### Y2H screens

The coding sequence for full-length MEL-26 (GenBank accession no. gi:212645231) was PCR amplified and cloned into the pB27 plasmid as a C-terminal fusion to LexA (N-LexA-MEL-26-C). The construct was checked by sequencing the entire insert and used as a bait to screen separately two random-primed *C. elegans* cDNA libraries constructed into the pP6 plasmid. The first library was constructed by combining equimolar amounts of mRNA from four different N2 samples: (1) males and hermaphrodites (all stages including embryos), (2) starved mixed stage culture, (3) heat-shocked mixed stage culture, and (4) dauer stage. The second library was prepared mixed stage embryos isolated by bleaching. pB27 and pP6 derive from the original pBTM116 (Vojtek and Hollenberg, 1995) and pGADGH

(Bartel et al., 1993) plasmids, respectively. 138 million clones of the *C. elegans* embryo library (13-fold its complexity) were screened using a mating protocol as previously described (Fromont-Racine et al., 1997). In brief, L40ΔGal4 (*MATa*) yeasts transformed with the MEL-26 bait were mated with a single-use aliquot of Y187 (*MATα*) yeasts previously transformed with the embryo library and stored at −80°C. A total of 138 diploid His+ colonies were selected on a medium without tryptophan, leucine, and histidine. To handle MEL-26 mild autoactivation of the *His3* reporter gene, 2 mM 3-aminotriazole was added to the selective medium during the screening. Similarly, 112 million clones of the mixed stage library were screened in the presence of 5 mM 3-aminotriazole and yielded 76 His+ colonies. The interacting fragments recovered in the positive colonies were amplified by PCR, sequenced at both their 5′ and 3′ ends, and identified in GenBank. Finally, each interaction was assigned a confidence score as previously described (Formstecher et al., 2005).

### Mixed stage library (pool of three preparations)
**Unstressed mixed stage worms.** 30 N2 hermaphrodites were mated to an excess of males on large nematode growth media (NGM) plates. Worms were grown at 20°C for 4–5 d, harvested before food was exhausted, washed in water twice, and rapidly frozen in liquid nitrogen.

**"Stressed" mixed stage worms.** 30 N2 hermaphrodites were mated to an excess of males on large NGM plates. Worms were grown at 20°C for 4–5 d and then submitted to the following treatments: (a) starvation: worms were washed off food in M9 medium and incubated for 7 h at room temperature with agitation; (b) heat shock: worms were heat shocked for 1 h at 35°C and then allowed to recover at 20°C for 6 h. For both treatments, preparations were combined, washed in water twice, and rapidly frozen in liquid nitrogen.

**Dauer stage worms.** N2 hermaphrodites were grown in liquid culture at 22–25°C until cultures arrested in dauer stage. Debris and contaminants were removed by sucrose floatation.

### Embryo library
N2 hermaphrodites were grown in liquid culture at 20°C until a significant number of gravid adults were present. Worms were then settled on ice and plated on large NGM plates for several hours. Plates were then washed with water. 30 ml of worm suspension supplemented with 10 ml bleach and 2.5 ml of 10 N NaOH were incubated with shaking until worms were disintegrated. After two cycles of ice-cold water washing and centrifugation at 1,000 *g* for 4 min at 4°C, the embryos were rapidly frozen in liquid nitrogen.

### Confidence score for the Y2H screens
Predicted biological score scores have been shown to positively correlate with the biological significance of interactions (Rain et al., 2001; Wojcik et al., 2002). Two different levels of analysis are used to compute the predicted biological score. A local score is first determined based on the independence and redundancy of the interacting fragments. For overlapping prey fragments, the distribution of reading frames and stop codons is also considered. A global score is then computed using the interactions identified in all the screens performed on the same library at Hybrigenics. This global score is determined as the probability of an interaction to be nonspecific. Score categories have been created for ease of use, from A (highest confidence) to D (lowest confidence). Interactions with prey domains previously found in >10 distinct screens performed on the same *C. elegans* libraries are specifically flagged with an E confidence score. Finally, the F category tags known false-positives of the technique.

### Data submission to external databases
The protein interactions from this publication have been submitted to the IMEx (http://www.imexconsortium.org/) consortium through IntAct and assigned the identifier IM-20907.

The entire results of both MEL-26 Y2H screens can be browsed using the PIMRider software at http://pimr.hybrigenics.com.

### Online supplemental material
Fig. S1 shows ASPM-1 and PPFR-1 protein localization in meiotic embryos. Fig. S2 shows wild-type MI versus MII divisions. Table S1 is a list of partners identified by the Y2H screens performed using MEL-26 as bait. Online supplemental material is available at http://www.jcb.org/cgi/content/full/jcb.201304174/DC1. Additional data are available in the JCB DataViewer at http://dx.doi.org/10.1083/jcb.201304174.dv.

## References

Bartel, P.L., and C.-T. Chien. R. Sternglanz, and S. Fields. 1993. Using the two-hybrid system to detect protein-protein interactions. *In* Cellular Interactions in Development: A Practical Approach. D.A. Hartley, editor. Oxford University Press, Oxford. 153–179.

Brenner, S. 1974. The genetics of *Caenorhabditis elegans*. *Genetics*. 77:71–94.

Clark-Maguire, S., and P.E. Mains. 1994. Localization of the mei-1 gene product of *Caenorhaditis elegans*, a meiotic-specific spindle component. *J. Cell Biol.* 126:199–209. http://dx.doi.org/10.1083/jcb.126.1.199

Dow, M.R., and P.E. Mains. 1998. Genetic and molecular characterization of the *Caenorhabditis elegans* gene, mel-26, a postmeiotic negative regulator of mei-1, a meiotic-specific spindle component. *Genetics*. 150:119–128.

Dumont, J., and A. Desai. 2012. Acentrosomal spindle assembly and chromosome segregation during oocyte meiosis. *Trends Cell Biol.* 22:241–249. http://dx.doi.org/10.1016/j.tcb.2012.02.007

Dumont, J., K. Oegema, and A. Desai. 2010. A kinetochore-independent mechanism drives anaphase chromosome separation during acentrosomal meiosis. *Nat. Cell Biol.* 12:894–901. http://dx.doi.org/10.1038/ncb2093

Fabritius, A.S., M.L. Ellefson, and F.J. McNally. 2011. Nuclear and spindle positioning during oocyte meiosis. *Curr. Opin. Cell Biol.* 23:78–84. http://dx.doi.org/10.1016/j.ceb.2010.07.008

Formstecher, E., S. Aresta, V. Collura, A. Hamburger, A. Meil, A. Trehin, C. Reverdy, V. Betin, S. Maire, C. Brun, et al. 2005. Protein interaction mapping: a *Drosophila* case study. *Genome Res.* 15:376–384. http://dx.doi.org/10.1101/gr.2659105

Fromont-Racine, M., J.C. Rain, and P. Legrain. 1997. Toward a functional analysis of the yeast genome through exhaustive two-hybrid screens. *Nat. Genet.* 16:277–282. http://dx.doi.org/10.1038/ng0797-277

Furukawa, M., Y.J. He, C. Borchers, and Y. Xiong. 2003. Targeting of protein ubiquitination by BTB-Cullin 3-Roc1 ubiquitin ligases. *Nat. Cell Biol.* 5:1001–1007. http://dx.doi.org/10.1038/ncb1056

Han, X., J.E. Gomes, C.L. Birmingham, L. Pintard, A. Sugimoto, and P.E. Mains. 2009. The role of protein phosphatase 4 in regulating microtubule severing in the *Caenorhabditis elegans* embryo. *Genetics*. 181:933–943. http://dx.doi.org/10.1534/genetics.108.096016

Hartman, J.J., J. Mahr, K. McNally, K. Okawa, A. Iwamatsu, S. Thomas, S. Cheesman, J. Heuser, R.D. Vale, and F.J. McNally. 1998. Katanin, a microtubule-severing protein, is a novel AAA ATPase that targets to the centrosome using a WD40-containing subunit. *Cell*. 93:277–287. http://dx.doi.org/10.1016/S0092-8674(00)81578-0

Kamath, R. S., M. Martinez-Campos, P. Zipperlen, A.G. Fraser, and J. Ahringer. 2001. Effectiveness of specific RNA-mediated interference through ingested double-stranded RNA in *Caenorhabditis elegans*. *Genome Biol.* 2:RESEARCH0002.

Kemphues, K.J., N. Wolf, W.B. Wood, and D. Hirsh. 1986. Two loci required for cytoplasmic organization in early embryos of *Caenorhabditis elegans*. *Dev. Biol.* 113:449–460. http://dx.doi.org/10.1016/0012-1606(86)90180-6

Kitagawa, D., C. Busso, I. Flückiger, and P. Gönczy. 2009. Phosphorylation of SAS-6 by ZYG-1 is critical for centriole formation in *C. elegans* embryos. *Dev. Cell.* 17:900–907. http://dx.doi.org/10.1016/j.devcel.2009.11.002

Kurz, T., L. Pintard, J.H. Willis, D.R. Hamill, P. Gönczy, M. Peter, and B. Bowerman. 2002. Cytoskeletal regulation by the Nedd8 ubiquitin-like protein modification pathway. *Science*. 295:1294–1298. http://dx.doi.org/10.1126/science.1067765

Loughlin, R., J.D. Wilbur, F.J. McNally, F.J. Nédélec, and R. Heald. 2011. Katanin contributes to interspecies spindle length scaling in *Xenopus*. *Cell*. 147:1397–1407. http://dx.doi.org/10.1016/j.cell.2011.11.014

Lu, C., M. Srayko, and P.E. Mains. 2004. The *Caenorhabditis elegans* microtubule-severing complex MEI-1/MEI-2 katanin interacts differently with two superficially redundant beta-tubulin isotypes. *Mol. Biol. Cell.* 15:142–150. http://dx.doi.org/10.1091/mbc.E03-06-0418

Mains, P.E., K.J. Kemphues, S.A. Sprunger, I.A. Sulston, and W.B. Wood. 1990. Mutations affecting the meiotic and mitotic divisions of the early *Caenorhabditis elegans* embryo. *Genetics*. 126:593–605.

McNally, K.P., and F.J. McNally. 2011. The spindle assembly function of *Caenorhabditis elegans* katanin does not require microtubule-severing activity. *Mol. Biol. Cell*. 22:1550–1560. http://dx.doi.org/10.1091/mbc.E10-12-0951

McNally, F.J., and R.D. Vale. 1993. Identification of katanin, an ATPase that severs and disassembles stable microtubules. *Cell*. 75:419–429. http://dx.doi.org/10.1016/0092-8674(93)90377-3

McNally, K., A. Audhya, K. Oegema, and F.J. McNally. 2006. Katanin controls mitotic and meiotic spindle length. *J. Cell Biol*. 175:881–891. http://dx.doi.org/10.1083/jcb.200608117

O'Rourke, S.M., C. Carter, L. Carter, S.N. Christensen, M.P. Jones, B. Nash, M.H. Price, D.W. Turnbull, A.R. Garner, D.R. Hamill, et al. 2011. A survey of new temperature-sensitive, embryonic-lethal mutations in *C. elegans*: 24 alleles of thirteen genes. *PLoS ONE*. 6:e16644. http://dx.doi.org/10.1371/journal.pone.0016644

Pintard, L., T. Kurz, S. Glaser, J.H. Willis, M. Peter, and B. Bowerman. 2003a. Neddylation and deneddylation of CUL-3 is required to target MEI-1/Katanin for degradation at the meiosis-to-mitosis transition in *C. elegans. Curr. Biol*. 13:911–921. http://dx.doi.org/10.1016/S0960-9822(03)00336-1

Pintard, L., J.H. Willis, A. Willems, J.L. Johnson, M. Srayko, T. Kurz, S. Glaser, P.E. Mains, M. Tyers, B. Bowerman, and M. Peter. 2003b. The BTB protein MEL-26 is a substrate-specific adaptor of the CUL-3 ubiquitin-ligase. *Nature*. 425:311–316. http://dx.doi.org/10.1038/nature01959

Rain, J.C., L. Selig, H. De Reuse, V. Battaglia, C. Reverdy, S. Simon, G. Lenzen, F. Petel, J. Wojcik, V. Schächter, et al. 2001. The protein-protein interaction map of *Helicobacter pylori*. *Nature*. 409:211–215. http://dx.doi.org/10.1038/35051615

Sambrook, J., E.F. Fristch, and T. Maniatis. 1989. Molecular cloning: a laboratory manual. Second edition. Cold Spring Harbor Laboratory Press, Cold Spring harbor, NY. 626 pp.

Srayko, M., D.W. Buster, O.A. Bazirgan, F.J. McNally, and P.E. Mains. 2000. MEI-1/MEI-2 katanin-like microtubule severing activity is required for *Caenorhabditis elegans* meiosis. *Genes Dev*. 14:1072–1084.

Srayko, M., E.T. O'toole, A.A. Hyman, and T. Müller-Reichert. 2006. Katanin disrupts the microtubule lattice and increases polymer number in *C. elegans* meiosis. *Curr. Biol*. 16:1944–1949. http://dx.doi.org/10.1016/j.cub.2006.08.029

Stitzel, M.L., J. Pellettieri, and G. Seydoux. 2006. The *C. elegans* DYRK kinase MBK-2 marks oocyte proteins for degradation in response to meiotic maturation. *Curr. Biol*. 16:56–62. http://dx.doi.org/10.1016/j.cub.2005.11.063

van der Voet, M., C.W. Berends, A. Perreault, T. Nguyen-Ngoc, P. Gönczy, M. Vidal, M. Boxem, and S. van den Heuvel. 2009. NuMA-related LIN-5, ASPM-1, calmodulin and dynein promote meiotic spindle rotation independently of cortical LIN-5/GPR/Galpha. *Nat. Cell Biol*. 11:269–277. http://dx.doi.org/10.1038/ncb1834

Vojtek, A.B., and S.M. Hollenberg. 1995. Ras-Raf interaction: two-hybrid analysis. *Methods Enzymol*. 255:331–342. http://dx.doi.org/10.1016/S0076-6879(95)55036-4

Wojcik, J., I.G. Boneca, and P. Legrain. 2002. Prediction, assessment and validation of protein interaction maps in bacteria. *J. Mol. Biol*. 323:763–770. http://dx.doi.org/10.1016/S0022-2836(02)01009-4

Xu, L., Y. Wei, J. Reboul, P. Vaglio, T.H. Shin, M. Vidal, S.J. Elledge, and J.W. Harper. 2003. BTB proteins are substrate-specific adaptors in an SCF-like modular ubiquitin ligase containing CUL-3. *Nature*. 425:316–321. http://dx.doi.org/10.1038/nature01985

Yang, H.Y., K. McNally, and F.J. McNally. 2003. MEI-1/katanin is required for translocation of the meiosis I spindle to the oocyte cortex in *C. elegans*. *Dev. Biol*. 260:245–259. http://dx.doi.org/10.1016/S0012-1606(03)00216-1